Dirk Grosenick 15.11.2021

# Generalized Self-Calibrating Probe Approach

## Contents



## 1 Introduction: the original self-calibrating probe design

Fig. 1 illustrates the NIRSPORT2 rectangular probe design with the two source positions S1 and S2 and the two detector positions DA and DB. The four detector signals $V_{1A}$, $V_{2A}$, $V_{1B}$ and $V_{2B}$ are measured sequentially. The short and long distances are $\rho_S$ = 30 mm and $\rho_L$ = 35 mm.

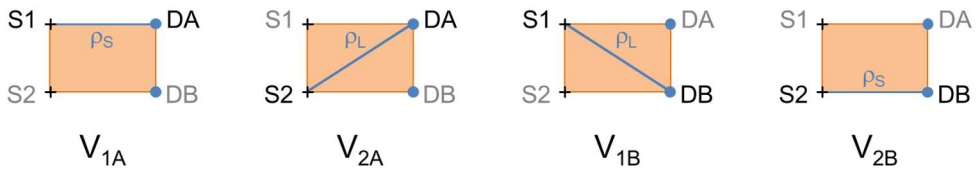


Fig. 1. Source-detector combinations for the self-calibrating probe measurement with rectangular probe design. $V_{1A}$, $V_{2A}$, $V_{1B}$ and $V_{2B}$ indicate the four measured voltages.

Using the self-calibrating probe approach of Hueber et al., the effective attenuation coefficient (also called slope) is calculated by the following equation:

$$\mu_{eff} = \left[\frac{1}{2}\ln\left(\frac{V_{1B}V_{2A}}{V_{1A}V_{2B}}\right) + 2\ln\left(\frac{\rho_L}{\rho_S}\right)\right] \Big/ \left(\rho_S - \rho_L\right) \qquad (1)$$

Basic assumptions for this equation are:

- semi-infinite medium with zero boundary condition (in reflection)
- $\rho \gg 1/\mu_s'$ (long distances) and $\rho \gg 1/\kappa$

## 2 Different source positions at the two wavelengths

In the real source design the two LEDs (760 nm and 850 nm) are located at different positions (Fig. 2a). Hence, the distances $\rho_S$ and $\rho_L$ depend on the source alignment. The calculation of $\mu_{eff}$ at the two

wavelengths, however, was done so far by assuming that $\rho_S$ and $\rho_L$ are the same for both wavelengths (which is of course not true!).

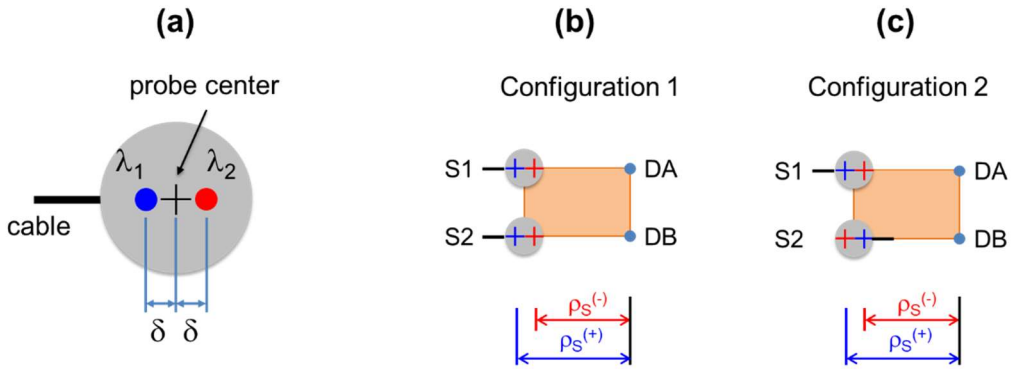


Fig. 2. (a) True source geometry with distance 2δ between the two LEDs. (b) Symmetric positioning of the source probes (configuration 1), (c) asymmetric positioning (configuration 2). The distances $\rho_S$ and $\rho_L$ (not shown) are different for both wavelengths then.

The experimental observation was, that a symmetric positioning of the source probes (configuration 1, Fig. 2b) yields wrong results for the oxygen saturation, whereas an asymmetric positioning gives apparently correct results (configuration 2, Fig. 2c). These observations are based on the fact that the analysis was done with the nominal distances instead of using the true distances.

In the following, both configurations and the reasons for failing or working are discussed in detail, together with a correct treatment of the problem.

## 3 Symmetric source positioning (Configuration 1)

A correct analysis for configuration 1 requires to acount for the different distances ρ for the two wavelengths. These distances are illustrated in Fig. 3. For wavelength 1 the distances $\rho_S^{(+)}$ and $\rho_L^{(+)}$ have to be taken into accout, for wavelength 2 the distances: $\rho_S^{(-)}$ and $\rho_L^{(-)}$ accordingly.

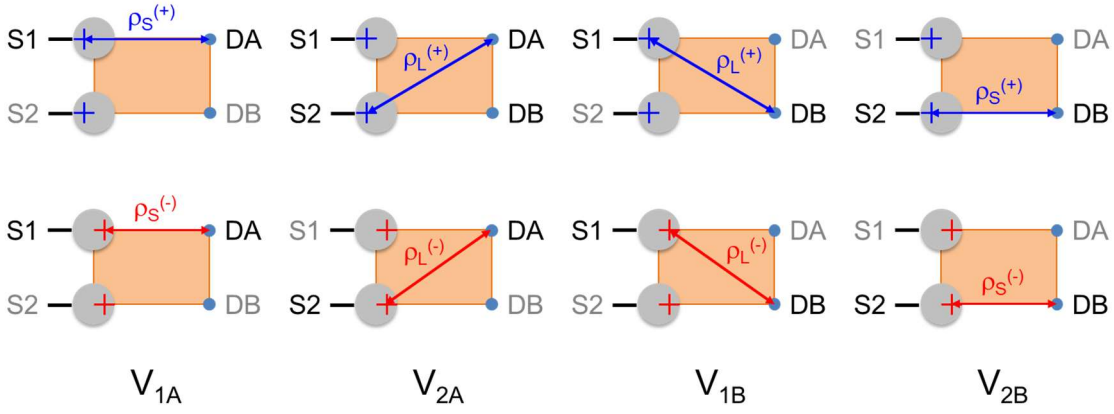


Fig. 3. Source-detector distances for configuration 1 for the two wavelengths (top row: wavelength 1, bottom row: wavelength 2)

The correct equations for calculation of $\mu_{eff}$ are:

$$\mu_{eff}(\lambda_1)=\left[\frac{1}{2}\ln\left(\frac{V_{1B}(\lambda_1)V_{2A}(\lambda_1)}{V_{1A}(\lambda_1)V_{2B}(\lambda_1)}\right)+2\ln\left(\frac{\rho_L^{(+)}}{\rho_S^{(+)}}\right)\right]\Big/\left(\rho_S^{(+)}-\rho_L^{(+)}\right) \quad (2)$$

$$\mu_{eff}(\lambda_2)=\left[\frac{1}{2}\ln\left(\frac{V_{1B}(\lambda_2)V_{2A}(\lambda_2)}{V_{1A}(\lambda_2)V_{2B}(\lambda_2)}\right)+2\ln\left(\frac{\rho_L^{(-)}}{\rho_S^{(-)}}\right)\right]\Big/\left(\rho_S^{(-)}-\rho_L^{(-)}\right) \quad (3)$$

Saturation values obtained on the basis of Eqs. (2) and (3) are correct then as will be illustrated below in Fig. 4.

In the present study on phantom C2 the nominal $\rho$ values were applied in the analysis, which corresponds to the following equations:

$$\mu_{eff}(\lambda_1)=\left[\frac{1}{2}\ln\left(\frac{V_{1B}\left(\lambda_1,\rho_L^{(+)}\right)V_{2A}\left(\lambda_1,\rho_L^{(+)}\right)}{V_{1A}\left(\lambda_1,\rho_S^{(+)}\right)V_{2B}\left(\lambda_1,\rho_S^{(+)}\right)}\right)+2\ln\left(\frac{\rho_L}{\rho_S}\right)\right]\Big/\left(\rho_S-\rho_L\right) \quad (4)$$

$$\mu_{eff}(\lambda_2)=\left[\frac{1}{2}\ln\left(\frac{V_{1B}\left(\lambda_2,\rho_L^{(-)}\right)V_{2A}\left(\lambda_2,\rho_L^{(-)}\right)}{V_{1A}\left(\lambda_2,\rho_S^{(-)}\right)V_{2B}\left(\lambda_2,\rho_S^{(-)}\right)}\right)+2\ln\left(\frac{\rho_L}{\rho_S}\right)\right]\Big/\left(\rho_S-\rho_L\right) \quad (5)$$

To compare the results for Eqs. (2,3) vs. Eqs. (4,5) reflectance profiles from a Monte Carlo simulation are used assuming the known optical properties of phantom C2. The simulations are based on a source displacement of $2\delta$ = 1 mm (see Fig. 2). Conversion from $\mu_{eff}$ to $\mu_a$ was done by applying the known values of $\mu_s$'. The oxygen saturation values calculated from $\mu_a(\lambda)$ are based on an assumed water fraction of 75% which is equivalent to the present NIRSPORT2 analysis algorithm.

Fig. 4 shows that Eqs. (2) and (3) yield a correct result whereas for Eqs. (4) and (5) the derived saturation goes strongly up, when the 760 nm LED is farer away from the detectors, or strongly down, when the 850 nm LED is farer from the detectors. The solid lines in Fig. 4 present the reference properties used as input for the MC simulation.

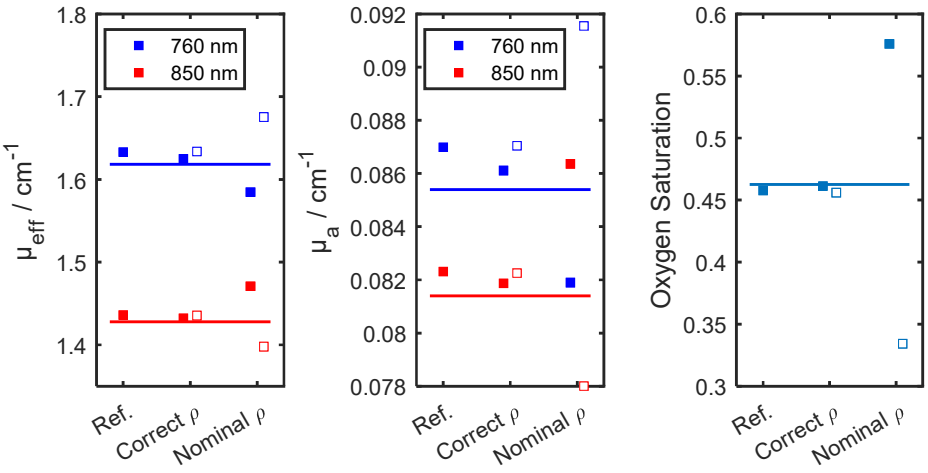


Fig. 4. Comparison of $\mu_{eff}$, $\mu_a$, and $StO_2$ for configuration 1.

- „Correct ρ" = analysis using the correct Eqs. (2) and (3)
- „Nominal ρ" = analysis using the wrong Eqs. (4) and (5)
- „Ref." = source with both LEDs assumed at the same position (Eq. (1))

The filled symbols for „Correct" and „Nominal" represent results for 760 nm being far from the detectors, the open symbols the result for 850 nm being far from the detectors. The lines represent the input parameters for the MC simulation.

## 4 Anti-symmetric source positioning (Configuration 2)

The anti-symmetric configuraton 2 (see Fig. 2c) violates a basic assumption of Eq. (1), the equal source-detector distances for cross-wise measurements (at a single wavelength), like e.g. $V_{1A}(\lambda_1)$and $V_{2B}(\lambda_1)$. The analysis of the present measurements on phantom C2 with NIRSPORT2 was done by using the nominal values $\rho_L$ and $\rho_S$ similar to the symmetric configuration in Sect. 3. In other words, $\mu_{eff}(\lambda_1)$ and $\mu_{eff}(\lambda_2)$ were calculated from the following equations (6) and (7):

$$\mu_{eff}(\lambda_1) = \left[\frac{1}{2}\ln\left(\frac{V_{1B}\left(\lambda_1,\rho_L^{(+)}\right)V_{2A}\left(\lambda_1,\rho_L^{(-)}\right)}{V_{1A}\left(\lambda_1,\rho_S^{(+)}\right)V_{2B}\left(\lambda_1,\rho_S^{(-)}\right)}\right)+2\ln\left(\frac{\rho_L}{\rho_S}\right)\right]\Big/\left(\rho_S-\rho_L\right) \tag{6}$$

$$\mu_{eff}(\lambda_2) = \left[\frac{1}{2}\ln\left(\frac{V_{1B}\left(\lambda_2,\rho_L^{(-)}\right)V_{2A}\left(\lambda_2,\rho_L^{(+)}\right)}{V_{1A}\left(\lambda_2,\rho_S^{(-)}\right)V_{2B}\left(\lambda_2,\rho_S^{(+)}\right)}\right)+2\ln\left(\frac{\rho_L}{\rho_S}\right)\right]\Big/\left(\rho_S-\rho_L\right) \tag{7}$$

In Eq. (6) the first term is a good approximation for the required term with the nominal lengths:

$$\frac{V_{1B}\left(\lambda_2,\rho_L^{(-)}\right)V_{2A}\left(\lambda_2,\rho_L^{(+)}\right)}{V_{1A}\left(\lambda_2,\rho_S^{(-)}\right)V_{2B}\left(\lambda_2,\rho_S^{(+)}\right)} \approx \frac{V_{1B}\left(\lambda_2,\rho_L\right)V_{2A}\left(\lambda_2,\rho_L\right)}{V_{1A}\left(\lambda_2,\rho_S\right)V_{2B}\left(\lambda_2,\rho_S\right)} \tag{8}$$

The same holds true for Eq. (7) when compared to Eq. (1). Hence, Eqs. (6) and (7) are good approximations of Eq. (1) for both wavelengths, and reasonable saturation values are obtained. Fig. 5 shows the results for $\mu_{eff}$, $\mu_a$ and $StO_2$ based on the same simulation assumptions underlying Fig. 4.

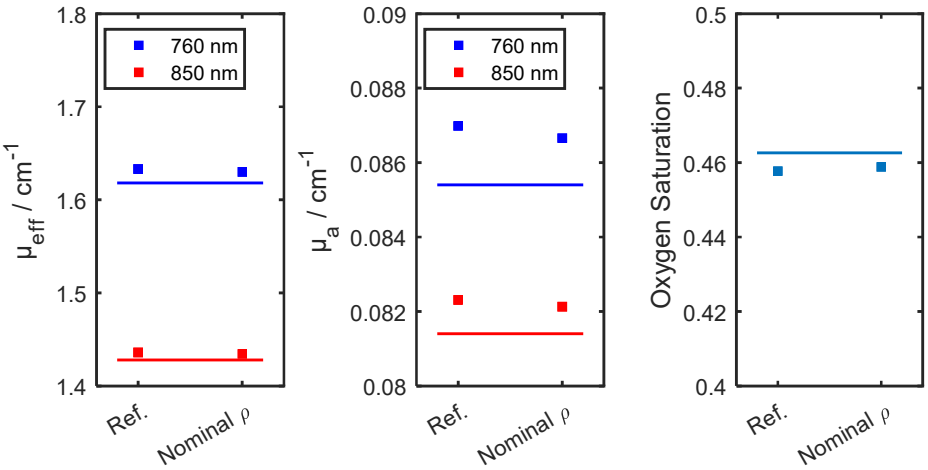


Fig. 5. Comparison of $\mu_{eff}$, $\mu_a$, and $StO_2$ for configuration 2. The lines represent the input parameters for the MC simulation.

For the anti-symmetric configuration exact formulas can be derived as well by following the general framework in the next section.

## 5 Generalized self-calibrating probe approach

The self-calibrating probe approach can be extended to arbitrary source-detector distances. Of course, the various source-detector combinations should sample the same tissue region to have a constant $\mu_{eff}$ (assumption of a homogeneous medium).

Start point is the following expression for the flux density J for the semi-infinite homogeneous medium in reflection at a selected distance ρ to the point-like source (which is the basis for Eq. (1) above):

$$J(\rho) \approx \frac{A_0 z_0}{2\pi} \frac{exp(-\mu_{eff}\rho)}{\rho^2} \mu_{eff} \tag{8}$$

The measured voltage V is related to J by the two factors S and D accounting for the source strength, detector sensitivity, acceptance angles etc.

With two sources S1, S2 and two detectors DA, DB we get four measurements (at a single wavelength). The source-detector distances are denoted as $\rho_1$, $\rho_2$, $\rho_3$ and $\rho_4$. Fig. 6 gives an example for arbitrary distribution of the four components.

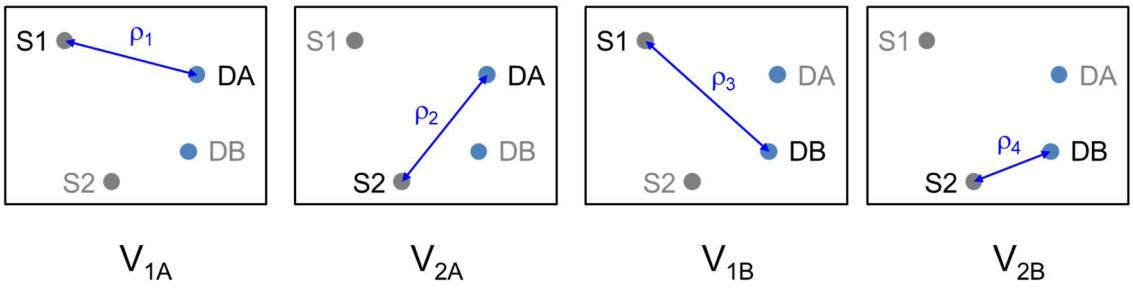


Fig. 6. Arbitrary source-detector arrangement with the four measurements $V_{1A}$ to $V_{2B}$

The four measured voltages are given by the following equations:

$$V_{1A} = S_1 D_A J(\rho_1) = S_1 D_A \frac{A_0 z_0}{2\pi} \frac{exp(-\mu_{eff}\rho_1)}{\rho_1^2} \mu_{eff} \tag{8}$$

$$V_{2A} = S_2 D_A J(\rho_2) = S_2 D_A \frac{A_0 z_0}{2\pi} \frac{exp(-\mu_{eff}\rho_2)}{\rho_2^2} \mu_{eff} \tag{9}$$

$$V_{1B} = S_1 D_B J(\rho_3) = S_1 D_B \frac{A_0 z_0}{2\pi} \frac{exp(-\mu_{eff}\rho_3)}{\rho_3^2} \mu_{eff} \tag{10}$$

$$V_{2B} = S_2 D_B J(\rho_4) = S_2 D_B \frac{A_0 z_0}{2\pi} \frac{exp(-\mu_{eff}\rho_4)}{\rho_4^2} \mu_{eff} \tag{11}$$

We can construct the basic ratio of measured voltages that becomes free of the source and detector factors $S_1$, $S_2$, $D_A$, and $D_B$, similar to the first term in Eq. (1):

$$\begin{aligned} \frac{V_{1B}V_{2A}}{V_{1A}V_{2B}} &= \frac{S_1 D_B \frac{A_0 z_0}{2\pi} \frac{exp(-\mu_{eff}\rho_3)}{\rho_3^2} \mu_{eff} \quad S_2 D_A \frac{A_0 z_0}{2\pi} \frac{exp(-\mu_{eff}\rho_2)}{\rho_2^2} \mu_{eff}}{S_1 D_A \frac{A_0 z_0}{2\pi} \frac{exp(-\mu_{eff}\rho_1)}{\rho_1^2} \mu_{eff} \quad S_2 D_B \frac{A_0 z_0}{2\pi} \frac{exp(-\mu_{eff}\rho_4)}{\rho_4^2} \mu_{eff}} \\ &= exp\left(\mu_{eff}(\rho_1 + \rho_4 - \rho_2 - \rho_3)\right) \frac{\rho_1^2 \rho_4^2}{\rho_2^2 \rho_3^2} \end{aligned} \tag{12}$$

Taking the logarithm yields:

$$\ln\left(\frac{V_{1B}V_{2A}}{V_{1A}V_{2B}}\right) = \mu_{eff}(\rho_1 + \rho_4 - \rho_2 - \rho_3) + 2\ln\left(\frac{\rho_1\rho_4}{\rho_2\rho_3}\right) \tag{13}$$

From this expression we get $\mu_{eff}$ as:

$$\mu_{eff} = \left(\ln\left(\frac{V_{1B}(\rho_3)V_{2A}(\rho_2)}{V_{1A}(\rho_1)V_{2B}(\rho_4)}\right) + 2\ln\left(\frac{\rho_2\rho_3}{\rho_1\rho_4}\right)\right) \Big/ (\rho_1 + \rho_4 - \rho_2 - \rho_3) \tag{14}$$

This is the generalized formulation of the self-calibrating probe approach. The distances $\rho_1$, $\rho_2$, $\rho_3$ and $\rho_4$ have to be inserted as realized in the experiments. The arguments of the voltages indicate the underlying distance according to Fig. 6.

Eq. (1) for the symmetric configuration is obtained from Eq. (14) by setting $\rho_1 = \rho_4 = \rho_S$ = and $\rho_2 = \rho_3 = \rho_L$. Similar, Eqs. (2) and (3) can be derived from Eq. (14).

For a correct treatment of the anti-symmetric configuration 2 shown in Fig. 7 (and discussed in Sect. 4) the four distances have to be taken according to Table 1. With these definitions correct saturation values are obtained (not shown here).

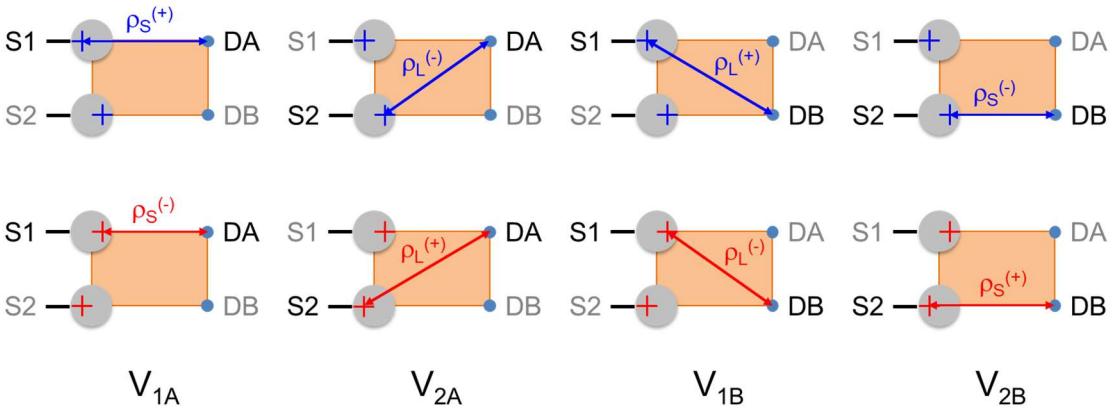


Fig. 7. Source-detector distances for configuration 2 for the two wavelengths (top row: wavelength 1, bottom row: wavelength 2)

| | $\lambda_1$ | $\lambda_2$ |
|---|---|---|
| $\rho_1$ | $\rho_S^{(+)}$ | $\rho_S^{(-)}$ |
| $\rho_2$ | $\rho_L^{(-)}$ | $\rho_L^{(+)}$ |
| $\rho_3$ | $\rho_L^{(+)}$ | $\rho_L^{(-)}$ |
| $\rho_4$ | $\rho_S^{(-)}$ | $\rho_S^{(+)}$ |

Tab. 1. Source-detector distances for configuration 2 for the two wavelengths to be used in Eq. (14)